Microsyst Technol (2018) 24:1733–1742
https://doi.org/10.1007/s00542-017-3548-9

TECHNICAL PAPER

Development of a novel long range piezoelectric motor based on double rectangular trajectories driving

Shupeng Wang[1] · Weibin Rong[1] · Lefeng Wang[1] · Zhichao Pei[1] · Hui Xie[1] · Lining Sun[1]

Received: 31 July 2017 / Accepted: 28 August 2017 / Published online: 2 September 2017

Abstract This paper proposes a novel stepping type piezoelectric motor that can perform long range rotational motion with high resolution. Pseudo-rigid-body method is used to establish the kinematics model of the driving mechanism and analyze the motion trajectory of the driving foot. The static deformation of the driving mechanism is simulated by finite element analysis. In experiments, a motor prototype is fabricated and its performance is tested by the established experimental system. The results indicate that the motor prototype can work stably step by step and all steps have high reproducibility. The prototype can achieve 331.2 μrad maximum stepping angle at the driving voltage of 150 V and driving frequency of 1 Hz. The minimum stable stepping angle and the maximum output torque are 1.47 μrad and 76.44 mNm, respectively. The maximum angular velocity of the motor prototype is about 37,662.1 μrad/s when the driving voltage is 150 V and the driving frequency is 128 Hz. By applying proper driving voltage and frequency, the proposed piezoelectric motor can produce a satisfactory angular velocity.

1 Introduction

With the rapid development of science research and industry, there is a wide range of requirement of the high-accuracy positioners with nanometer resolution and millimeter stroke, which could guarantee higher quality products and research facilities (Ye et al. 2013; Zhang et al. 2012; Kang and Kim 2013; Rong et al. 2017; Ho and Jan 2016; Chen et al. 2016). Piezoelectric materials are a kind of non-traditional materials operated by the inverse piezoelectric effect of the ceramic element and the fictional coupling between the interfaces (Liu et al. 2016a, b; Zhu et al. 2016). Given the significance of simple structures with high stiffness and rapid response, no coil and magnet, high power under small weight, high precision locating in nanometer, the piezoelectric materials are applied in various nanopositioning systems (Zhu et al. 2016; Liu et al. 2016b; Zhang et al. 2011; Ru et al. 2010).

While having so many advantages, piezoelectric materials' small working stroke considerably limits their applications (Liu et al. 2016a, b; Zhu et al. 2016; Wang et al. 2016, 2017a; Sharp et al. 2010). Therefore, the development of piezoelectric motors combining both long range and high resolution has been a challenging topic, and attracted the attention of many researchers in the last decades (Wang et al. 2016, 2017a; Sharp et al. 2010; Aloufi et al. 2016).

At present several methods have been proposed to obtain long motion range of the piezoelectric materials (Shutov et al. 2005; Peng et al. 2015; Wang et al. 2015; Clark et al. 2016; Li et al. 2013, 2014, 2015a; Lobontiu et al. 2001; Wang et al. 2017b). Due to the simplified structure and high resolution, the flexure hinge amplification mechanism is one of the popular methods (Wang et al. 2015; Clark et al. 2016). Nevertheless, their working ranges are usually less than dozens to hundreds of micrometers, which is still not enough for the cross-scale system. Thereupon, the stepping type piezoelectric motors are developed (Li et al. 2013, 2014, 2015a, b; Lobontiu et al. 2001; Wang et al. 2017b; Zhang et al. 2008; Rakotondrabe

✉ Weibin Rong
rwb@hit.edu.cn

✉ Hui Xie
xiehui@hit.edu.cn

[1] State Key Laboratory of Robotics and System, Harbin Institute of Technology, Harbin 150080, Heilongjiang, China

et al. 2009; Aoyagi et al. 2004; Yang et al. 2016; Shao et al. 2016; Liu et al. 2016c). These types of piezoelectric motors can move step by step and their working range can reach to millimeters, even endless. So far, the stepping type piezoelectric motors mainly include inchworm type motors (Li et al. 2013, 2014, 2015a, b; Lobontiu et al. 2001), stick–slip type motors (Wang et al. 2017b; Zhang et al. 2008; Rakotondrabe et al. 2009) and ultrasonic type motors (Aoyagi et al. 2004; Yang et al. 2016; Shao et al. 2016; Liu et al. 2016c).

The inchworm motor is a type of bionic device with one feeding unit and two clamping units. By imitating the movement of the inchworm, the inchworm motor can output long range motion (Li et al. 2013, 2014, 2015a; Lobontiu et al. 2001). The stick–slip motor usually consists of an inertial module. When the inertial module moves forward slowly, the rotor/mover can be driven by the frictional force. But when the inertial module moves backward rapidly, the rotor/mover cannot follow the fast motion of the inertial module and remains in place due to its inertia (Wang et al. 2017b; Zhang et al. 2008; Li et al. 2015b; Rakotondrabe et al. 2009). The ultrasonic motor is equipped with a stator that can generate an elliptical driving trajectory on a driving point. By the elliptical driving trajectory, the rotor/mover which is placed against the driving point can be then driven (Aoyagi et al. 2004; Yang et al. 2016; Shao et al. 2016; Liu et al. 2016c). Table 1 presents the advantages and disadvantages of the three types of piezoelectric motors and the performance data of several reviewed piezoelectric motors are summarized in Table 2.

This study proposes a novel stepping type piezoelectric motor based on two synchronous feet driving. The motor is equipped with an octagonal driving mechanism which is constituted by two driving feet and eight right circular flexure hinges. With the help of two piezo-stacks, the two driving feet can move synchronously and generate two synchronous rectangular motion trajectories to drive the rotor to deliver unlimited range rotary motion. Comparing with current piezoelectric motors, the designed motor possesses the following characteristics: (1) the motor is equipped with only two piezo-stacks to generate two synchronous rectangular motions of the two driving feet; (2) using two synchronous motions of the two driving feet to drive the rotor can contribute to reducing the loads of the bearings; (3) driving by two synchronous feet are beneficial to obtain large output torque of the motor.

Table 1 Advantages and disadvantages of piezoelectric motors

Type	Advantage	Disadvantage
Inchworm	Large output torque	Complex control
	High resolution	Low speed
Stick–slip	Compact structure	Small output torque
	Simple control	Reverse displacement
Ultrasonic	High speed	Low resolution
	Compact structure	Heat generation

2 Structure and working principle

2.1 Structure of the motor

The configuration of the designed piezoelectric motor with specific dimensions of 100 mm × 50 mm × 40 mm is shown in Fig. 1. The piezoelectric motor mainly consists of a stator, a rotor, two piezo-stacks, two adjusting bolts and two sets of preload units. The rotor can be served as the rotating stage to output torques and rotations. Two precision bearings and two bearing seats are utilized to support the rotor. The preload units which are constituted by two preload bolts and two preload rings are used to hold the position of the rotor during the whole rotation process. As the core component of the motor, the stator illustrated in Fig. 2 is made up of two sets of guiding flexure hinges, two piezo-stack installing grooves and a driving mechanism which is constituted by two driving feet and eight right circular flexure hinges. The whole stator is made of 65 Mn for good elastic property of the flexure hinges. The two piezo-stacks are nested inside the piezo-stack installing grooves and preloaded by two adjusting bolts. In addition to preloading the piezo-stacks, the adjusting bolts are also utilized to adjust the clearances between the driving feet and the rotor. It should be paid more attention to assemble the rotor, since the position of the rotor will influence the performance of the motor. So after assembling, the rotor should be placed in the middle of the two driving feet.

2.2 Working principle of the motor

Figure 1 presents that two piezo-stacks which are named piezo-stack A and piezo-stack B are installed in two sides of the stator. As illustrated in Fig. 3, two triangular wave signal voltages with phase difference of $\pi/2$ are applied to the piezo-stacks A and B. Figure 3 also presents the displacement inputs A and B of the driving mechanism.

In this study, an octagonal driving mechanism with two driving feet and eight right circular flexure hinges is designed. When the piezo-stacks obtain power, they are stretched and push the driving mechanism to deform and move in accordance with certain laws. As Fig. 4 shows, pseudo-rigid-body method is used to establish the motion model to describe the working principle of the motor. The right circular flexure hinges are assumed to have only one degree of freedom for rotational deformation and they are

Table 2 Performance of reviewed piezoelectric motors

References	Type	Velocity (μrad/s)	Output (mNm)	Resolution (μrad)
(Li et al. 2013)	Inchworm	6.51×10^3	93.1	4.95
(Li et al. 2015a)	Inchworm	3.52×10^3	294	0.23
(Wang et al. 2017b)	Stick–slip	1.17×10^3	70.6	1.83
(Zhang et al. 2008)	Stick–slip	3.35×10^3	20	1.0
(Aoyagi et al. 2004)	Ultrasonic	8.38×10^8	0.06	N/A
(Yang et al. 2016)	Ultrasonic	3.58×10^7	6.26	N/A

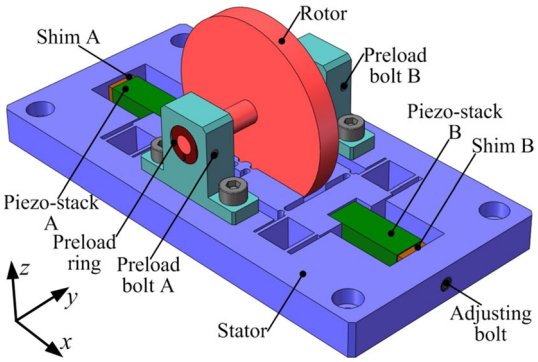

Fig. 1 Schematic diagram of the motor

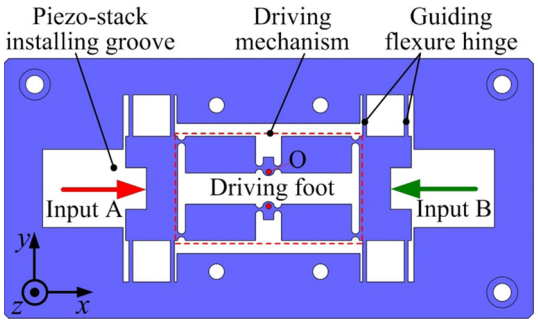

Fig. 2 Structure of the stator

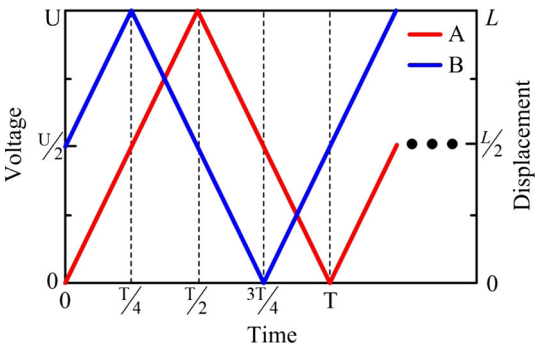

Fig. 3 Signal and displacement inputs

simulated by a combination of a rotation pair and a torsion spring. The guiding flexure hinges are simulated by a combination of a translation pair and an extension spring.

The moving process of the proposed motor in a working cycle can be divided into five steps described as follows:

1. As shown in Fig. 4a, at time 0, the voltages applied to piezo-stacks A and B are 0 and U/2 respectively and the output displacements of the piezo-stacks A and B are 0 and *L*/2 respectively. So the displacement inputs of the driving mechanism A and B are 0 and *L*/2 respectively. The two driving feet are located in the left and do not contact the rotor.
2. As shown in Fig. 4b, at time T/4, the voltages applied to piezo-stacks A and B are U/2 and U respectively and the output displacements of the piezo-stacks A and B are *L*/2 and *L* respectively. So the displacement inputs of the driving mechanism A and B are *L*/2 and *L* respectively. The two driving feet move toward each other simultaneously and clamp the rotor. This process can be called the clamping motion.
3. As shown in Fig. 4c, at time T/2, the voltages applied to the piezo-stacks A and B are U and U/2 respectively and the output displacements of the piezo-stacks A and B are *L* and *L*/2 respectively. So the displacement inputs of the driving mechanism A and B are *L* and *L*/2 respectively. The two driving feet move to the right simultaneously and rotate the rotor anticlockwise by a small angle α. This process can be called the feeding motion.
4. As shown in Fig. 4d, at time 3T/4, the voltages applied to the piezo-stacks A and B are U/2 and 0 respectively and the output displacements of the piezo-stacks A and B are *L*/2 and 0 respectively. So the displacement inputs of the driving mechanism A and B are *L*/2 and 0 respectively. The two driving feet move opposite each other simultaneously and unclamp the rotor. This process can be called the unclamping motion.
5. As shown in Fig. 4a, at time T, the voltages applied to the piezo-stacks A and B are 0 and U/2 respectively and the output displacements of the piezo-stacks A and B are 0 and *L*/2 respectively. So the displacement inputs of the driving mechanism A and B are 0 and *L*/2 respectively. The two driving feet move to the left simultaneously and do not contact the rotor. This process can be called the resetting motion.

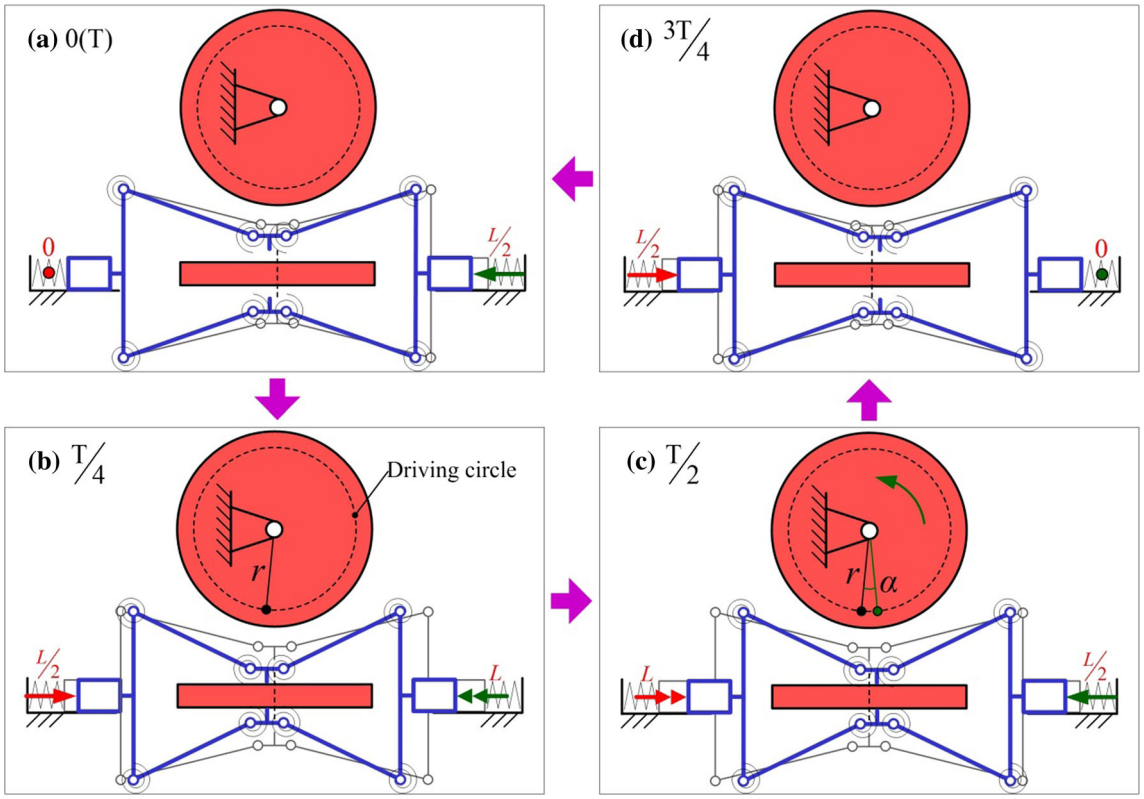

Fig. 4 Working principle sequential diagrams

As Fig. 4 illustrates, after clamping motion, feeding motion, unclamping motion and resetting motion, the proposed piezoelectric motor rotates one step. By repeating steps (1)–(5), the piezoelectric motor can output unlimited range rotary motion step by step. Moreover, reverse motion of the piezoelectric motor can be obtained if the phase difference of two triangular wave signal voltages is changed from π/2 to 3π/2.

3 Model and analysis

3.1 Analysis of driving mechanism

As mentioned in Sect. 2.2, the driving mechanism is an octagonal structure with two driving feet and eight right circular flexure hinges and pseudo-rigid-body method is used to establish the motion model. As shown in Fig. 5, the motion model is established based on only a quarter of the driving mechanism since the structure is symmetrical. The right circular flexure hinges are simulated by rotation pairs and the guiding flexure hinges are simulated by translation pairs (the torsion spring and extension spring are omitted in kinematic analysis).

In Fig. 5, according to the Pythagorean theorem, the following relationships can be obtained:

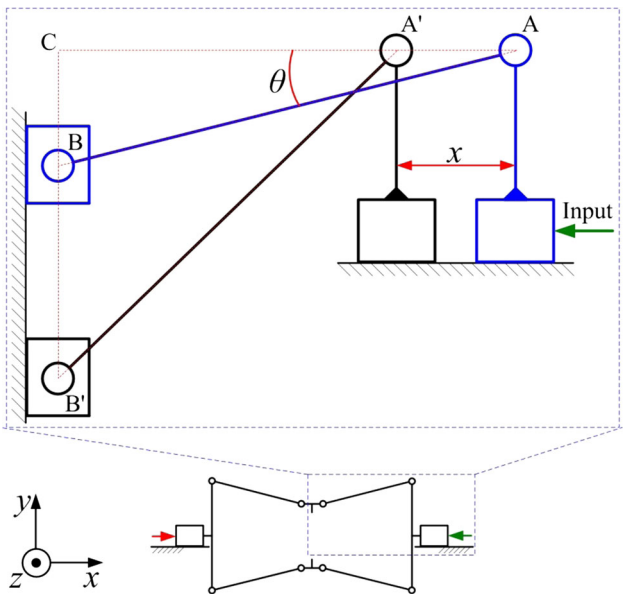

Fig. 5 Analysis of driving mechanism

$$\begin{cases} l_{AC}^2 + l_{BC}^2 = l_{AB}^2 \\ l_{A'C}^2 + l_{B'C}^2 = l_{A'B'}^2 \end{cases} \quad (1)$$

where l_{AC} is the length of the segment AC and so on.

According to the geometric relationship, the following equations can be got:

$$\begin{cases} l_{AC} = l_{A'C} + x \\ l_{AB} = l_{A'B'} \end{cases} \tag{2}$$

Insert Eq. (2) into the Eq. (1) and the following equation can be got:

$$l_{B'C} = \sqrt{l_{AB}^2 - (l_{AB}\cos\theta - x)^2} \tag{3}$$

According to the geometric relationship, the following equation can be got:

$$l_{BB'} = l_{B'C} - l_{BC} \tag{4}$$

Inserting Eq. (3) into the Eq. (4), the distance between the Points B and B' can be obtained:

$$l_{B'C} = \sqrt{l_{AB}^2 - (l_{AB}\cos\theta - x)^2} - l_{AB}\sin\theta \tag{5}$$

3.2 Trajectory analysis of the driving foot

As shown in Fig. 6, the model is established based on half of the driving mechanism to analyze the trajectory of the upper driving foot. According to the Eq. (5), the distance between the points O and O′ in y direction can be obtained by the following equation:

$$y_{OO'} = \sqrt{l_{AB}^2 - \left(l_{AB}\cos\theta - \frac{x_A + x_B}{2}\right)^2} - l_{AB}\sin\theta \tag{6}$$

In addition, the distance between the points O and O′ in x direction can be obtained by the following equation:

$$x_{OO'} = -\frac{x_A - x_B}{2} \tag{7}$$

According to Eqs. (6) and (7), if there is no constraint from the rotor, the coordinates of the upper driving foot in steps a–d (see Sect. 2.2) can be got by the following equations, respectively:

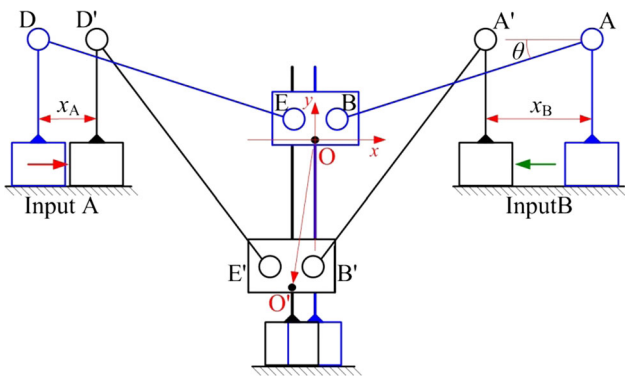

Fig. 6 Trajectory analysis of the driving foot

$$\begin{cases} x_a = -\dfrac{L}{4} \\ y_a = l_{AB}\sin\theta - \sqrt{l_{AB}^2 - \left(l_{AB}\cos\theta - \dfrac{L}{4}\right)^2} \end{cases} \tag{8}$$

$$\begin{cases} x_b = -\dfrac{L}{4} \\ y_b = l_{AB}\sin\theta - \sqrt{l_{AB}^2 - \left(l_{AB}\cos\theta - \dfrac{3L}{4}\right)^2} \end{cases} \tag{9}$$

$$\begin{cases} x_c = \dfrac{L}{4} \\ y_c = l_{AB}\sin\theta - \sqrt{l_{AB}^2 - \left(l_{AB}\cos\theta - \dfrac{3L}{4}\right)^2} \end{cases} \tag{10}$$

$$\begin{cases} x_d = \dfrac{L}{4} \\ y_d = l_{AB}\sin\theta - \sqrt{l_{AB}^2 - \left(l_{AB}\cos\theta - \dfrac{L}{4}\right)^2} \end{cases} \tag{11}$$

So the displacement of the feeding motion (see Sect. 2.2) can be calculated by the following equation:

$$s = x_c - x_b = \frac{L}{2} \tag{12}$$

The designed values of l_{AB} and θ are 15.81 mm and 18.43°. The tested value of L is about 10.9 μm when the driving voltage and frequency are 150 V and 1 Hz. Inserting the values above into Eqs. (8)–(11), the motion trajectory of the upper driving foot can be obtained in Fig. 7. Inserting the value of L into the Eq. (12), the displacement of the feeding motion can be got:

$$s \approx 5.45\ \mu\text{m} \tag{13}$$

The radius r of the driving circle (see Fig. 4) is 16 mm. So the stepping angle of the proposed piezoelectric motor can be calculated:

$$\alpha \approx \frac{s}{r} \approx 340.6\ \mu\text{rad} \tag{14}$$

4 Simulation

By the finite element analysis, simulation of the driving mechanism is conducted to verify the theoretical results in Sect. 3. As shown in Fig. 8, the model of the stator is simplified to facilitate the calculation. Body sizing of 0.5 mm is used to refine the meshes. The elastic modulus and poisson ratio of the selected material 65 Mn are set to be 211 GPa and 0.288, respectively (Wang et al. 2017a). As Fig. 8 illustrates, the eight surfaces of the guiding flexure hinges are fixed and different displacement load

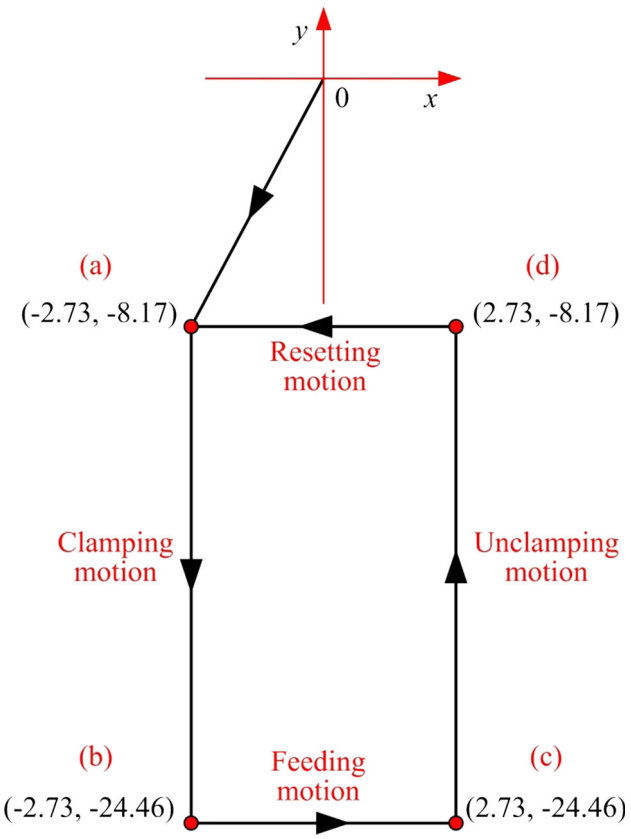

Fig. 7 Trajectory of the upper driving foot

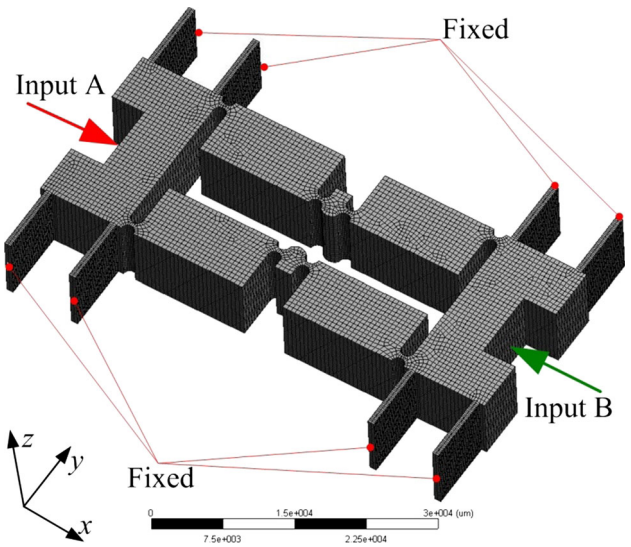

Fig. 8 The meshed model

combinations (shown in Fig. 9) are applied on the driving mechanism.

The total deformation status at every step is shown in Fig. 9. According to the simulation results, the coordinates of the upper driving foot in steps a–d (see Sect. 2.2) can be obtained:

$$\begin{aligned} &\text{(a) } (-2.66, -7.89) \quad \text{(d) } (2.66, -7.89) \\ &\text{(b) } (-2.66, -23.67) \quad \text{(c) } (2.66, -23.67) \end{aligned} \tag{15}$$

There are small differences between the theoretical results and the simulation results. This may be because that the deformation points are not exactly in the middle of the right circular flexure hinges.

5 Experiment

5.1 Experimental system and testing principle

A prototype of the motor is manufactured and a series of experiments are conducted via the established experimental system shown in Fig. 10. The experimental system mainly consists of one industry personal computer (IPC), one signal generator, one signal amplifier, one capacitance micrometer and the motor prototype. Two piezo-stacks (AE0707d18 from NEC-Tokin) with dimensions of $7 \times 7 \times 18$ mm^3 are utilized in the motor prototype. The working flowchart of the experimental system is illustrated in Fig. 11. When the system works, the control module in the IPC orders the signal generator to produce suitable voltage signals. Then the signal amplifier with 30× amplification ratio amplifies the signals to drive the motor prototype. At the same time, the capacitance micrometer with 0.375 nm measuring resolution and 500 μm maximum measuring range is used to measure the displacement between the capacitive sensor and a reflector attached on the rotor, which is presented in Fig. 12. The angular displacement of the rotor can be calculated approximately by the following equation when it is very small:

$$\Delta\varphi \approx \frac{\Delta l}{d} \tag{16}$$

where Δl is the measured value and d is the distance between the measured point and the rotational center of the rotor. At last, the IPC gathers and manages all data.

5.2 Experiment and discussion

The working performance of the piezoelectric motor prototype under 150 V driving voltage and 1 Hz driving frequency is presented in Fig. 13. When the signal voltages are applied, the rotor rotates stepwise, resulting in a large stroke rotary motion. The motor prototype has a stable operation and all steps have high reproducibility, which indicates that at every step, all of the clamping motion, feeding motion, unclamping motion and resetting motion (see Sect. 2.2) are in good operation state. The angular displacement of the rotor in one step can be called the stepping angle and its tested value is about 331.2 μrad

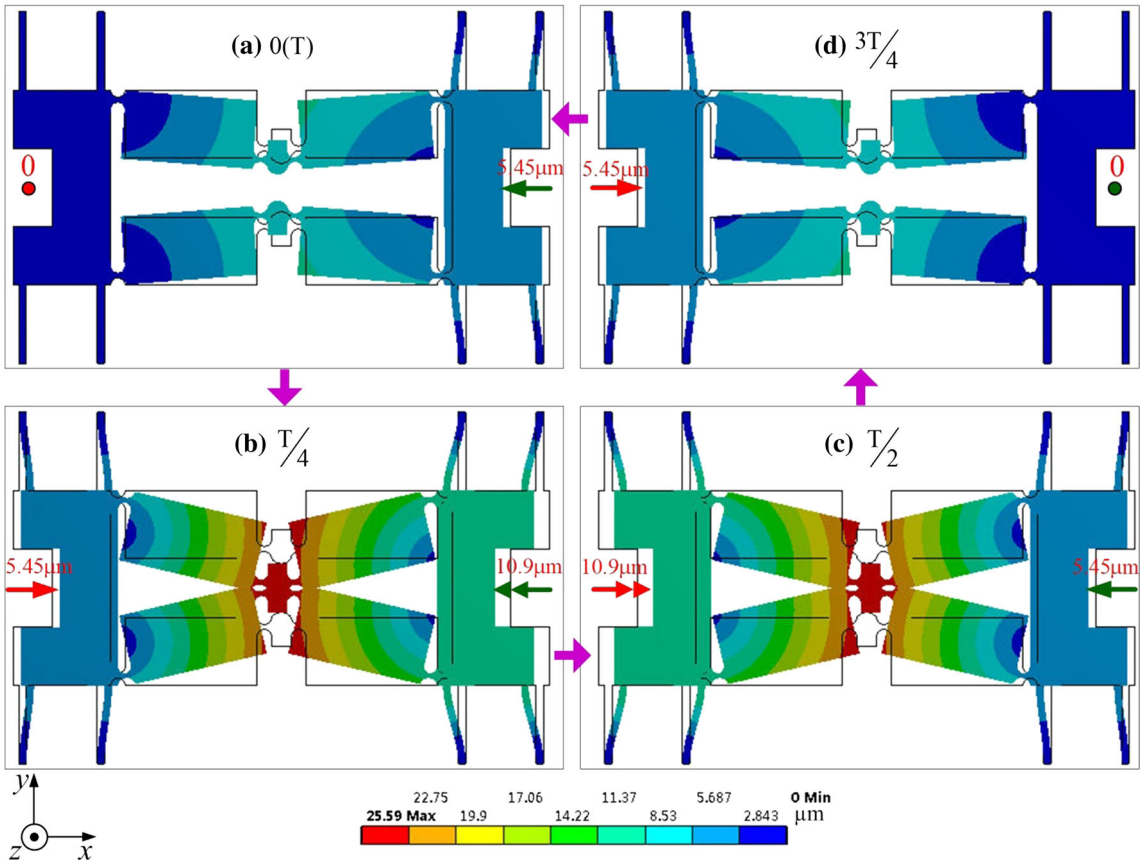

Fig. 9 Deformation status at every step

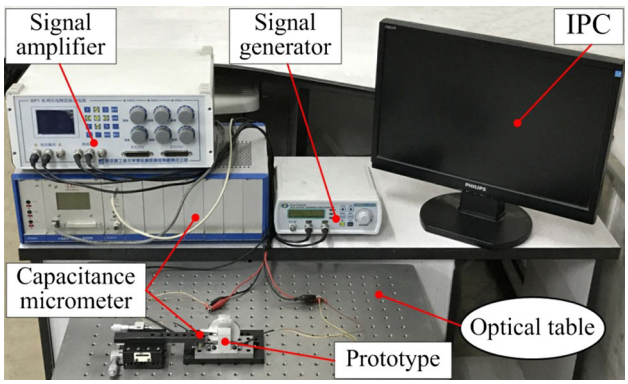

Fig. 10 Experimental system

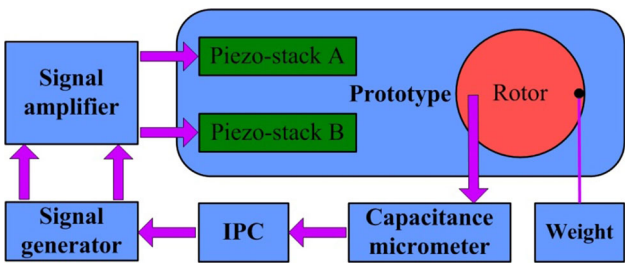

Fig. 11 Working flowchart of the experimental system

under 150 V driving voltage and 1 Hz driving frequency. It is slightly smaller than the theoretical value of 340.6 μrad. The possible reason may be that due to the manufacture and assembly errors, the actual radius of the driving circle is larger than the designed value of 16 mm. Because it is the line contact between the driving feet and the rotor, the driving circle may be not exactly at the midpoints of the contact segments.

If the stepping angle is tested, the angular velocity can be calculated by the following equation:

$$v = p \cdot f \tag{17}$$

where p is the value of the stepping angle and f is the frequency of the driving signals. With decreasing of the driving voltage, the elongation of the piezo-stacks decreases and according to the Eq. 14, the stepping angle of the piezoelectric motor also decreases and according to Eq. 17, the angular velocity of the piezoelectric motor also decreases if the driving frequency is constant. Under driving frequency of 1 Hz, the relationship between the angular velocity and driving voltage is shown in Fig. 14. The given frequency is 1 Hz because it is easy to observe and control when the motor works at this frequency. As Fig. 14 presents, there is approximate linear relationship

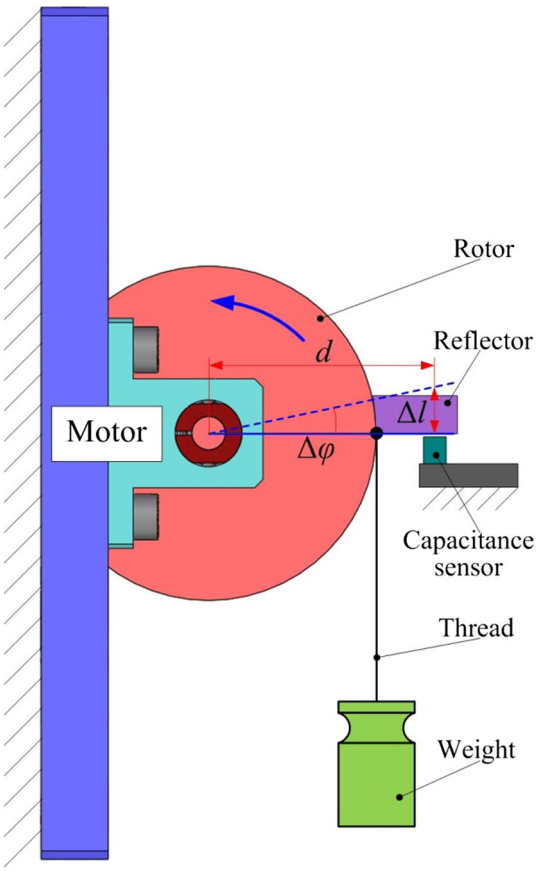

Fig. 12 Testing principle

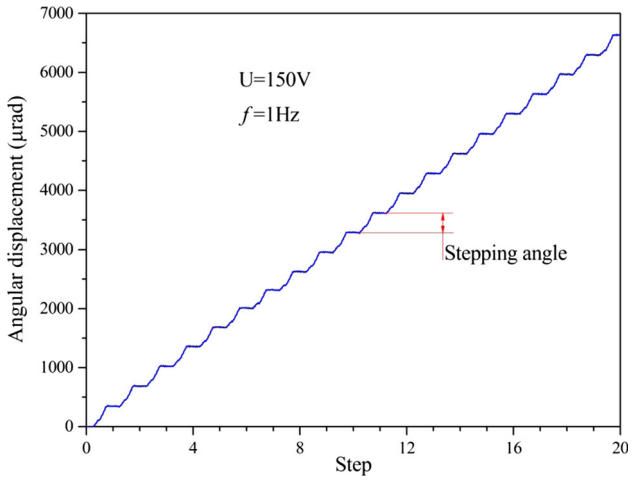

Fig. 13 Output under 150 V voltage and 1 Hz frequency

between the angular velocity and the driving voltage. The maximum angular velocity of the piezoelectric motor is about 331.2 μrad/s when the driving voltage is 150 V. When the driving voltage is 60 V, the angular velocity is 98.1 μrad/s. So if the driving frequency is fixed, we can obtain a satisfactory angular velocity by applying a proper driving voltage on the piezoelectric motor.

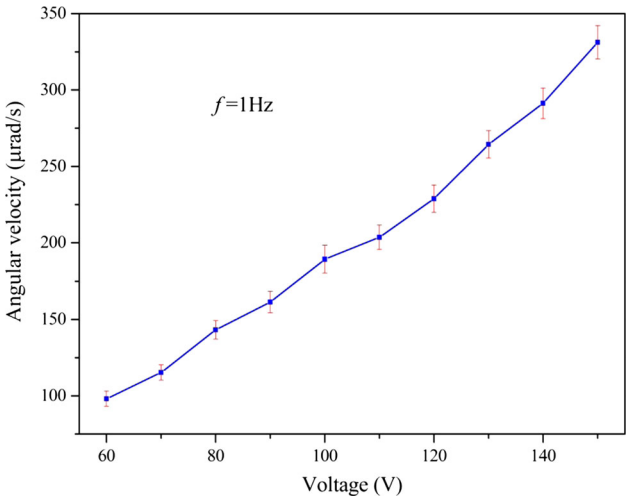

Fig. 14 Angular velocity under various driving voltages

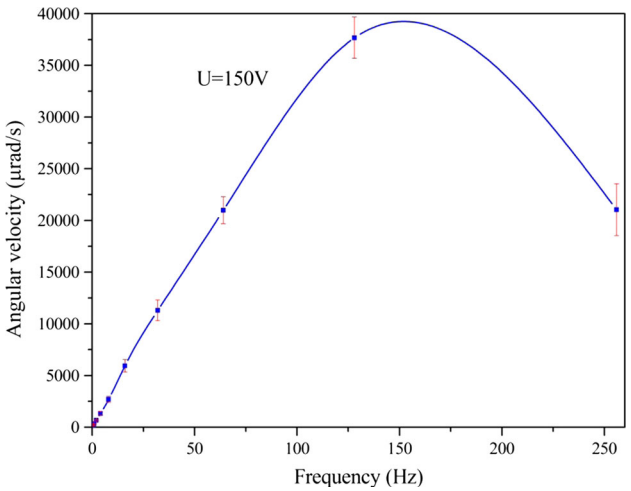

Fig. 15 Angular velocity under various driving frequencies

According to Eq. 17, we can also conclude that if the stepping angle is constant, the angular velocity of the piezoelectric motor increases with the increasing of the driving frequency. Figure 15 shows the relationship between the angular velocity of the motor and the driving frequency when the driving voltage is 150 V. When the driving frequency is less than 128 Hz, there is good relationship between the angular velocity and driving frequency. This indicates that the stepping angle of the piezoelectric motor is stable. However the angular velocity decreases when the driving frequency is more than 150 Hz. This indicates that the stepping angle of the piezoelectric motor decreases under high driving frequency. The possible reason may be that the response speed of the driving mechanism cannot follow with that of the driving signals under high frequency. Another possible reason is that the relative sliding between the driving foot and the rotor

increases with the increasing of the driving frequency. The maximum angular velocity of the piezoelectric motor is about 37,662.1 μrad/s when the driving frequency is 128 Hz. Similarly, when the driving voltage is fixed, a satisfactory angular velocity can be obtained if a proper driving frequency is applied on the piezoelectric motor.

For a precision motor, the minimum stable stepping angle which can be called the motion resolution is important. According to the analysis above, the stepping angle of the piezoelectric motor decreases with decreasing of the driving voltage when the driving frequency is constant. So we can test the minimum stable stepping angle by reducing the driving voltage. A series of experimental results indicates that the motor prototype cannot work stably if the driving voltage is less than 25 V. This may be caused by the clearances of the bearings and another possible reason is that the clamping forces are too small to drive the rotor at low driving voltage. So the motor cannot work stably. As Fig. 16 shows, a final angular displacement of 73.37 μrad is obtained after 50 cycle steps of the motor under 25 V driving voltage and 1 Hz driving frequency. The average stepping angle is about 1.47 μrad, which can be regarded as the motion resolution of the prototype. The negative displacement at every step may be caused by the clearances and the internal forces of the bearings.

Maximum output torque is one of the key parameters for a motor during real applications. In order to test the maximum output torque of the motor prototype, weights of different masses are attached on the rotor by an inelastic thread, which is shown in Fig. 12. The given driving voltage and frequency are 150 V and 1 Hz respectively in the tests. Figure 17 shows the relationship between the angular velocity and the weight attached. With increasing of the weight attached on the rotor, the angular velocity of the motor prototype decreases and there is approximate

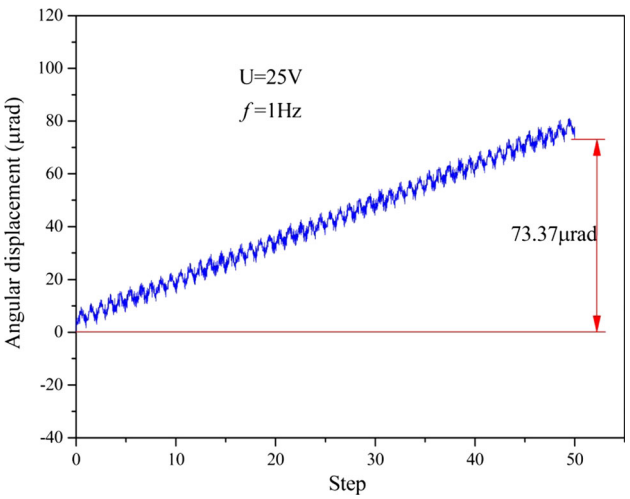

Fig. 16 Output in resolution test

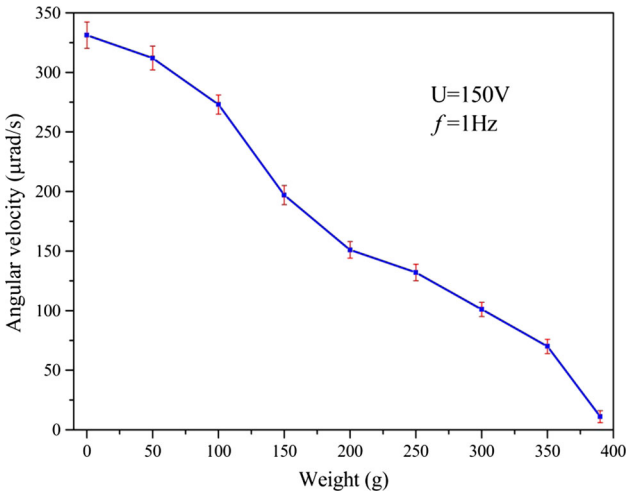

Fig. 17 Output torque test

linear relationship between the angular velocity and the weight. When the weight is more than 390 g, the motor prototype cannot work effectively. So the maximum output torque of the motor prototype is about 76.44 mNm.

6 Conclusion

This study presents a novel stepping type piezoelectric motor. The motor is equipped with an octagonal driving mechanism which is constituted by two driving feet and eight right circular flexure hinges. With the help of two piezo-stacks, the two driving feet can move synchronously and generate two synchronous rectangular motion trajectories to drive the rotor to deliver unlimited range rotary motion step by step. The mechanical structure and the working principle are discussed. The motion model of the driving mechanism is established by utilizing pseudo-rigid-body method and the motion trajectory of the driving foot is analyzed in theory. The static deformation of the driving mechanism is simulated by finite element analysis. In order to investigate the performance of the proposed piezoelectric motor, a prototype is fabricated and a set of experimental system is established. The experimental results demonstrate that the motor prototype can be operated stably step by step and all steps have high reproducibility. The motor can achieve 331.2 μrad maximum stepping angle when the driving voltage is 150 V and driving frequency is 1 Hz. The minimum stable stepping angle and the maximum output torque are 1.47 μrad and 76.44 mNm, respectively. The maximum angular velocity of the piezoelectric motor is about 37,662.1 μrad/s when the driving voltage is 150 V and the driving frequency is 128 Hz. By applying proper driving voltage and frequency, the designed piezoelectric motor can produce a satisfactory

angular velocity. Further studies will be performed to optimize the output performance and simplify the dimension of the proposed piezoelectric motor.

Acknowledgements This research is funded by the National Natural Science Foundation of China (51675141) and the Foundation for Innovative Research Groups of the National Natural Science Foundation of China (51521003) and Self-Planned Task of State Key Laboratory of Robotics and System (HIT) (SKLRS201709A).

References

Aloufi B, Behdinan K, Zu J (2016) Modeling and design of a high-performance hybrid actuator. Smart Mater Struct 25(12):125004

Aoyagi M, Suzuki F, Tomikawa Y et al (2004) High-speed thin ultrasonic spindle motor and its application. Jpn J Appl Phys 43(5S):2873

Chen C, Shi Y, Zhang J et al (2016) Novel linear piezoelectric motor for precision position stage. Chin J Mech Eng 29(2):378–385

Clark L, Shirinzadeh B, Zhong Y et al (2016) Design and analysis of a compact flexure-based precision pure rotation stage without actuator redundancy. Mech Mach Theory 105:129–144

Ho ST, Jan SJ (2016) A piezoelectric motor for precision positioning applications. Precis Eng 43:285–293

Kang BW, Kim J (2013) Design, fabrication, and evaluation of stepper motors based on the piezoelectric torsional actuator. IEEE/ASME Trans Mechatron 18(6):1850–1854

Li J, Zhao H, Qu H et al (2013) A piezoelectric-driven rotary actuator by means of inchworm motion. Sens Actuators A 194:269–276

Li J, Zhao H, Shao M et al (2014) Design and experiment performances of an inchworm type rotary actuator. Rev Sci Instrum 85(8):085004

Li J, Zhao H, Qu X et al (2015a) Development of a compact 2-DOF precision piezoelectric positioning platform based on inchworm principle. Sens Actuators A 222:87–95

Li J, Zhou X, Zhao H et al (2015b) Design and experimental performances of a piezoelectric linear actuator by means of lateral motion. Smart Mater Struct 24(6):065007

Liu Z, Yao Z, Li X et al (2016a) Design and experiments of a linear piezoelectric motor driven by a single mode. Rev Sci Instrum 87(11):115001

Liu Y, Yan J, Xu D et al (2016b) An I-shape linear piezoelectric actuator using resonant type longitudinal vibration transducers. Mechatronics 40:87–95

Liu Y, Yang X, Chen W et al (2016c) A bonded-type piezoelectric actuator using the first and second bending vibration modes. IEEE Trans Ind Electron 63(3):1676–1683

Lobontiu N, Goldfarb M, Garcia E (2001) A piezoelectric-driven inchworm locomotion device. Mech Mach Theory 36(4):425–443

Peng Y, Peng Y, Gu X et al (2015) A review of long range piezoelectric motors using frequency leveraged method. Sens Actuators A 235:240–255

Rakotondrabe M, Haddab Y, Lutz P (2009) Development, modeling, and control of a micro-/nanopositioning 2-dof stick–slip device. IEEE/ASME Trans Mechatron 14(6):733–745

Rong W, Liang S, Wang L et al (2017) Model and control of a compact long-travel accurate-manipulation platform. IEEE/ASME Trans Mechatron 22(1):402–411

Ru C, Zhang Y, Sun Y et al (2010) Automated four-point probe measurement of nanowires inside a scanning electron microscope. IEEE Trans Nanotechnol 10(4):674–681

Shao S, Shi S, Chen W et al (2016) Research on a linear piezoelectric actuator using T-shape transducer to realize high mechanical output. Appl Sci 6(4):103

Sharp SL, Paine JSN, Blotter JD (2010) Design of a linear ultrasonic piezoelectric motor. J Intell Mater Syst Struct 21(10):961–973

Shutov MV, Sandoz EE, Howard DL et al (2005) A microfabricated electromagnetic linear synchronous motor. Sens Actuators A 121(2):566–575

Wang F, Liang C, Tian Y et al (2015) Design of a piezoelectric-actuated microgripper with a three-stage flexure-based amplification. IEEE/ASME Trans Mechatron 20(5):2205–2213

Wang S, Rong W, Wang L et al (2016) Design, analysis and experimental performance of a stepping type piezoelectric linear actuator based on compliant foot driving. Smart Mater Struct 25(11):115003

Wang S, Rong W, Wang L et al (2017a) Design, analysis and experimental performance of a novel stick-slip type piezoelectric rotary actuator based on variable force couple driving. Smart Mater Struct 26(5):055005

Wang S, Rong W, Wang L et al (2017b) Design, analysis and experimental performance of a bionic piezoelectric rotary actuator. J Bionic Eng 14(2):348–355

Yang X, Liu Y, Chen W et al (2016) A cylindrical traveling wave ultrasonic motor using bonded-type composite beam. Ultrasonics 65:277–281

Ye X, Zhang Y, Ru C et al (2013) Automated pick-place of silicon nanowires. IEEE Trans Autom Sci Eng 10(3):554–561

Zhang H, Zeng P, Hua S et al (2008) Impact drive rotary precision actuator with piezoelectric bimorphs. Front Mech Eng China 3(1):71–75

Zhang Y, Liu X, Ru C et al (2011) Piezoresistivity characterization of synthetic silicon nanowires using a MEMS device. J Microelectromech Syst 20(4):959–967

Zhang YL, Li J, To S et al (2012) Automated nanomanipulation for nanodevice construction. Nanotechnology 23(6):065304

Zhu C, Chu X, Yuan S et al (2016) Development of an ultrasonic linear motor with ultra-positioning capability and four driving feet. Ultrasonics 72:66–72